

**CATTANEO-CHRISTOV HEAT FLUX AND HEAT
GENERATION/ABSORPTION EFFECT ON VISCOUS
WALTERS' B FLUID THROUGH A POROUS MEDIUM
WITH CHEMICAL REACTION**

B.J. AKINBO¹ AND B.I. OLAJUWON

ABSTRACT. The study of Walters' B fluid is essential in polymer materials processing which are useful in industries for the formation of plastic film and artificial fibers among others. In this paper, the significance of Cattaneo-Christov heat flux model on heat and mass transfer of a Walters B fluid through a medium porosity have been examined. The Cattaneo-Christov heat flux model was used to investigate the behaviours of heat transfer in the presence of Newtonian heating. The non-linear model equations for the study are re-worked into ordinary differential equations through exponential similarity transformation and executed via Homotopy Analysis Method. The obtained result were validated using Galerkin Weighted Residual method and good agreement is observed. Some of the major finding were that different values of the local Weissenberg Number enhances viscoelasticity of the fluid which reduces the motion of fluid and consequently thin momentum boundary layer thickness while various values of heat generation enhances the temperature field which enable the penetration of thermal effect to quiescent fluid.

Keywords and phrases: Cattaneo-Christov heat flux model, Viscous dissipation, Newtonian heating, Chemical Reaction, Homotopy Analysis Method.

2010 Mathematical Subject Classification: 35G61, 76D05 76N10, 78M25, 76W05

1. INTRODUCTION

The transport phenomenon via the electrical non-conducting fluid has been one of the most successful models to describe the behaviors of heat and mass transfer in many relevant situations. Recent development in the science and engineering field which focused on

Received by the editors May 24, 2021; Revised: September 28, 2021; Accepted: October 07, 2021

www.nigerianmathematicalsociety.org; Journal available online at <https://ojs.ictp.it/jnms/>

¹Corresponding author

higher molecular liquid shifted the attention of many researchers to the case of non-Newtonian fluid with vast industrial and scientific applications among which are lubrication systems, hydro-dynamical machines, and polymer processing. Keeping in mind the heat transfer phenomenon via Fourier's law of heat conduction, Hayat *et al.* [1-3] considered the impact of Cattaneo-Christov heat flux model on the different non-Newtonian models, such as Jeffrey liquid and Eyring-Powell fluid towards a stretching cylinder as well as Maxwell fluid over a stretching sheet with variable thickness. The result revealed among others that the temperature for Cattaneo-Christov heat flux model is less than the Fourier's expression. Dogonchi and Ganji [4] reported that the Nusselt number raises with the raising volume fraction of nanofluid and it abates with the ascending the radiation parameter while working on Cattaneo-Christov heat flux on buoyancy MHD nanofluid with the impact of Joule heating as well as thermal radiation. Shah *et al.* [5] worked on magnetohydrodynamics influence on the UCM fluid with Cattaneo-Christov heat flux model, where it was reported among others that the temperature declined with enhancement in Deborah number due to the reduction in time of deformation process. Mustafa [6] investigated upper-convected Maxwell fluid with Cattaneo-Christov heat flux model and the result perfectly agreed when compared with other numerical solutions. The velocity slip boundary condition is invoked by Han *et al.* [7] while investigating Maxwell fluid in the presence of Cattaneo-Christov heat flux model and it was reported that the elastic-force boosts heat transfer of the viscoelastic fluid. Kumar *et al.* [8] reported that the heat transfer rate of the flow past a cone is higher than that of the wedge flow while investigating MHD Cattaneo-Christov flow over a cone and a wedge with variable heat generation/absorption. UCM nanofluid flow across a melting surface is examined through Runge-Kutta-Fehlberg based shooting method with Cattaneo-Christov heat flux by Mahanthesh *et al.* [9] where the local Nusselt number declined with variation in Brownian motion and thermal stratification parameter. Ali and Sandeep [10] investigated MHD Casson-ferrofluid with the Cattaneo-Christov model for radiative heat transfer. The result indicated that the cone possesses a higher heat transfer rate in comparison with the flow over a wedge and a plate. Nadeem *et al.* [11] examined viscoelastic fluid with Cattaneo-Christov flux in the flow under the influence of Newtonian heating. Khan and Khan [12] worked on Burgers fluid via Cattaneo-Christov heat flux

model on three-dimensional flow while the Cattaneo-Christov heat flux impact is considered on Dogonchi and Ganji [13] through magnetohydrodynamics nanofluid flow via parallel plates. The result revealed that Nusselt number is an incrementing function of heat source but a diminishing function of the thermal relaxation parameter. The various values of Deborah number were found to magnify heat flux relaxation time by Abbasi and Shehzad [14] while working on Maxwell fluid via a three-dimensional flow, in the presence of temperature-dependent thermal conductivity. This enhanced heat flux relaxation time poses a reduction in the temperature but enhances the temperature gradient. Others researchers on the field like Liu *et al.* [15] and Kumar *et al.* [16] made their point in literature.

Taking into consideration the importance of heat and mass transport systems in the related disciplines and previous studies in the field, considerable attention has not been given to the influence of Cattaneo-Christov heat flux model in the flow of Walters' B fluid. On this note, this work is put together to examine the impact of Cattaneo-Christov heat flux model on a viscous Walters B fluid under the influence of Newtonian heating through an exponentially stretching sheet in the presence of heat generation/absorption and chemical reaction, which appeared on unaddressed in the literature to the best of our knowledge. The model equations executed via Homotopy Analysis method are compared with Galerkin Weighted Residual method for successful implementation of the numerical results.

2. FORMULATION

We examine a steady-case of an incompressible Walters' B fluid over an exponentially stretching sheet. The medium porosity is considered with electrically non-conducting fluid. The characteristic of heat transfer is executed in view of viscous dissipation and heat generation/absorption with Newtonian Heating while the mass transfer is considered with chemical reaction. The flow is confined in the region $y \geq 0$ in the presence of Cattaneo-Christov heat flux while the plate is assumed to be stretched with a velocity $U_w = U_0 \exp(x/l)$ along x - axis.

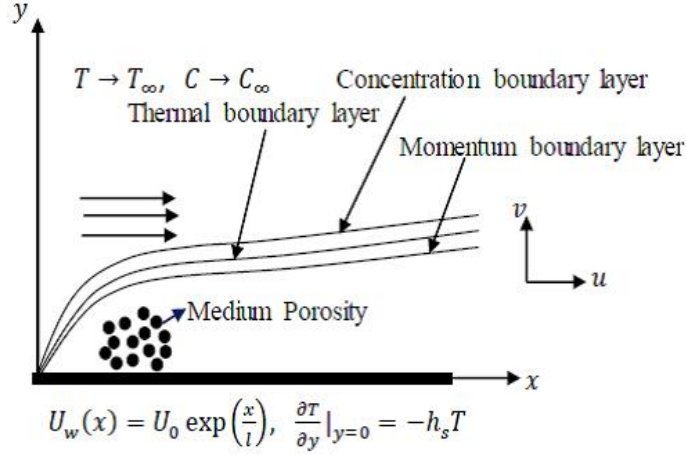


Fig. 1. Flow Geometry

Incorporating the assumption stated above, the model equations for transport phenomena of the studies under the boundary layer are considered as (Nandeppanavar *et al.* [17] and Hayat *et al.* [18])

$$\frac{\partial u}{\partial x} + \frac{\partial v}{\partial y} = 0 \quad (1)$$

$$u \frac{\partial u}{\partial x} + v \frac{\partial u}{\partial y} = \nu \frac{\partial^2 u}{\partial y^2} - \frac{\nu}{K} u - \frac{k_0}{\rho} \left[u \frac{\partial^3 u}{\partial x \partial y^2} + v \frac{\partial^3 u}{\partial x^3} + \frac{\partial u}{\partial x} \frac{\partial^2 u}{\partial y^2} - \frac{\partial u}{\partial y} \frac{\partial^2 u}{\partial x \partial y} \right] \quad (2)$$

$$u \frac{\partial T}{\partial x} + v \frac{\partial T}{\partial y} + \Gamma_E \Omega_E = \frac{k}{\rho C_p} \frac{\partial^2 T}{\partial y^2} + \frac{\nu}{C_p} \left(\frac{\partial u}{\partial y} \right)^2 - \frac{\delta k_0}{C_p} \left(\frac{\partial u}{\partial y} \right) \frac{\partial}{\partial y} \left[u \frac{\partial u}{\partial x} + v \frac{\partial u}{\partial y} \right] \quad (3)$$

$$u \frac{\partial C}{\partial x} + v \frac{\partial C}{\partial y} = D \frac{\partial^2 C}{\partial y^2} - r(C - C_\infty) \quad (4)$$

Notations (u, v) considered in (x, y) directions represent velocity components, Q_0 stands for heat generation/absorption coefficient, k_0 connotes elastic parameter, Γ_E stands for relaxation time of heat flux, ν presents kinematic viscosity, δ represents elastic-deformation, k symbolizes thermal conductivity, ρ denotes density, C_p body-forth

specific heat at constant pressure. Thus, Ω_E in energy Eq. (3) is defined as

$$\begin{aligned} \Omega_E = u \frac{\partial u}{\partial x} \frac{\partial T}{\partial x} + v \frac{\partial v}{\partial y} \frac{\partial T}{\partial y} + u^2 \frac{\partial^2 T}{\partial x^2} + v^2 \frac{\partial^2 T}{\partial y^2} + 2uv \frac{\partial^2 T}{\partial x \partial y} \\ + u \frac{\partial v}{\partial x} \frac{\partial T}{\partial y} + v \frac{\partial v}{\partial y} \frac{\partial T}{\partial x} \end{aligned} \quad (5)$$

Which are performed under the following domain

$$\begin{aligned} u(x, 0) = U_w(x) = U_0 \exp\left(\frac{x}{l}\right), \quad v(x, 0) = 0, \\ \frac{\partial T(x, 0)}{\partial x} = -h_s T, \quad C(x, 0) = C_w \end{aligned} \quad (6)$$

$$u \rightarrow 0, \quad T \rightarrow T_\infty, \quad C \rightarrow C_\infty \quad \text{as } y \rightarrow \infty \quad (7)$$

where, $T(> T_\infty)$ and $C(> C_\infty)$ symbolizes temperature and concentration of the fluid (ambient temperature and concentration), U_0 body-forth reference velocity, h_s pose heat transfer coefficient, l stands for characteristic length. The introduction of $u = \frac{\partial \psi}{\partial y}$ and $v = -\frac{\partial \psi}{\partial x}$ with the associated similarity-transformation techniques in line with (Khan [19])

$$\begin{aligned} \psi = \exp\left(\frac{x}{2l}\right) \sqrt{2\nu l U_0} f(\eta), \quad \eta = y \sqrt{\frac{U_0}{2\nu l}} \exp\left(\frac{x}{2l}\right), \\ u = U_0 \exp\left(\frac{x}{l}\right) f'(\eta), \quad v = -\sqrt{\frac{\nu U_0}{2l}} \exp\left(\frac{x}{2l}\right) [f(\eta) + \eta f'(\eta)] \\ \theta(\eta) = \frac{T - T_\infty}{T_\infty}, \quad \phi(\eta) = \frac{C - C_\infty}{C_w - C_\infty} \end{aligned} \quad (8)$$

on Eq. (1-7) result in non-dimensional equations of the form

$$\begin{aligned} \frac{d^3 f}{d\eta^3} + f(\eta) \frac{d^2 f}{d\eta^2} - 2 \left(\frac{df}{d\eta}\right)^2 - 2P_s \frac{df}{d\eta} \\ + We \left[\frac{3}{2} \left(\frac{d^2 f}{d\eta^2}\right)^2 - 3 \frac{df}{d\eta} \frac{d^3 f}{d\eta^3} + \frac{1}{2} f(\eta) \frac{d^4 f}{d\eta^4} \right] = 0 \end{aligned} \quad (9)$$

$$\begin{aligned} \frac{d^2\theta}{d\eta^2} + Pr f(\eta) \frac{d\theta}{d\eta} + Pr Ec \left(\frac{d^2 f}{d\eta^2} \right)^2 + Pr Q \theta(\eta) \\ - \frac{1}{2} \delta We Pr Ec \left[\frac{df}{d\eta} \left(\frac{d^2 f}{d\eta^2} \right)^2 - f(\eta) \frac{d^2 f}{d\eta^2} \frac{d^3 f}{d\eta^3} \right] \\ + \frac{1}{2} Pr \lambda_e \left(f(\eta) \frac{df}{d\eta} \frac{d\theta}{d\eta} - (f(\eta))^2 \frac{d^2 \theta}{d\eta^2} \right) = 0 \end{aligned} \quad (10)$$

$$\frac{d^2\phi}{d\eta^2} + Sc f(\eta) \frac{d\phi}{d\eta} - R Sc \phi(\eta) = 0 \quad (11)$$

with

$$\begin{aligned} \frac{df(\eta=0)}{d\eta} = 1, f(\eta=0) = 0, \\ \frac{d\theta(\eta=0)}{d\eta} = -\gamma(1 + \theta(\eta=0)), \phi(\eta=0) = 1 \end{aligned} \quad (12)$$

$$\frac{df(\eta \rightarrow \infty)}{d\eta} = 0, \theta(\eta \rightarrow \infty) = 0, \phi(\eta \rightarrow \infty) = 0 \quad (13)$$

where

$$\begin{aligned} Q = \frac{Q_0}{p C_p U_0}, Ps = \frac{\nu l}{K U_0}, We = \frac{k_0 U_w}{\rho \nu l}, Pr = \frac{\nu \rho C_p}{k} \\ \lambda_e = \frac{\Gamma_E U_w}{l}, \gamma = h_s \sqrt{\frac{2\nu l}{U_0}}, Ec = \frac{U_w^2}{C_p (T_\infty)} \end{aligned}$$

connote heat generation/absorption, Porosity parameter, local Weissenberg number, Prandtl number, thermal relaxation time, conjugate parameter for Newtonian heating and Eckert number respectively. The local Skin-friction, local Nusselt number and local Sherwood number are considered as

$$Cf = \frac{\tau_w}{\rho U_w^2}, Nu = \frac{x q_w}{k(T - T_\infty)}, Sh = \frac{x q_m}{D(C_w - C_\infty)} \quad (14)$$

with τ_w for shear stress on the plate, q_w stands for surface heat flux and q_m portray surface mass transfer which are defined as

$$\begin{aligned} \tau_w = \left[\mu \frac{\partial u}{\partial y} \right]_{y=0} - k_0 \left[u \frac{\partial^2 u}{\partial x \partial y} + v \frac{\partial^2 u}{\partial y^2} + \frac{\partial u}{\partial x} \frac{\partial u}{\partial y} \right]_{y=0}, \\ q_w = \left(-k \frac{\partial T}{\partial y} \right)_{y=0}, q_m = \left(-D \frac{\partial C}{\partial y} \right)_{y=0} \end{aligned} \quad (15)$$

Invoking (8) result in

$$\begin{aligned}
 Re_x^{\frac{1}{2}} C f_x &= \left(1 - \frac{7}{2} We\right) f''(0), \quad Re_x^{\frac{1}{2}} N u_x = \gamma \left(1 + \frac{1}{\theta(0)}\right), \\
 Re_x^{\frac{1}{2}} S h_x &= -\phi'(0) \quad (16)
 \end{aligned}$$

While $Re_x = \frac{cx^2}{\nu}$ body-forth local Reynolds number.

3. SOLUTION OF THE MODEL

Different methods like Adomial Decomposition, Differential Transform method, and shooting iteration technique together with Runge-Kutta and many more play an important role in providing solution to various forms of differential equations. Homotopy Analysis Method is utilized subject to its efficiency in addressing nonlinear differential equations. Invoking (12-13) in agreement with the procedure of solution (See Rashidi *et al.* [20]), we have

$$f_0(\eta) = 1 - \exp(-\eta), \quad \theta_0(\eta) = \frac{\gamma \exp(-\eta)}{(1 - \gamma)}, \quad \phi_0(\eta) = \exp(-\eta) \quad (17)$$

being the initial guess, while the linear operators L_f , L_θ and L_ϕ posed as;

$$\begin{aligned}
 L_f[f(\eta; r)] &= \frac{\partial^3 f(\eta; r)}{\partial \eta^3} - \frac{\partial f(\eta; r)}{\partial \eta}, \quad L_\theta[\theta(\eta; r)] = \frac{\partial^2 \theta(\eta; r)}{\partial \eta^2} - \theta(\eta; r), \\
 L_\phi[\phi(\eta; r)] &= \frac{\partial^2 \phi(\eta; r)}{\partial \eta^2} - \phi(\eta; r) \quad (18)
 \end{aligned}$$

are in accordance with

$$\begin{aligned}
 L_f[C_1 + C_2 \exp(\eta) + C_3 \exp(-\eta)] &= 0, \quad L_\theta[C_4 + C_5 \exp(-\eta)] = 0, \\
 L_\phi[C_6 + C_7 \exp(-\eta)] &= 0, \quad (19)
 \end{aligned}$$

where C_1, C_2, \dots, C_7 are constants

3.1. ZERO ORDER DEFORMATION PROBLEM

$$(1 - r)L_f[f(\eta; r) - f_0(\eta)] = r\hbar_f H_f(\eta) N_f[f(\eta; r)] \quad (20)$$

$$(1 - r)L_\theta[\theta(\eta; r) - \theta_0(\eta)] = r\hbar_\theta H_\theta(\eta) N_\theta[f(\eta; r), \theta(\eta; r)] \quad (21)$$

$$(1 - r)L_\phi[\phi(\eta; r) - \phi_0(\eta)] = r\hbar_\phi H_\phi(\eta) N_\phi[f(\eta; r), \phi(\eta; r)] \quad (22)$$

$$f(\eta = 0; r) = 0, \quad \frac{\partial f(\eta = 0; r)}{\partial \eta} = 1, \\ \frac{\partial \theta(\eta = 0; r)}{\partial \eta} = -\gamma [1 + \theta(\eta = 0; r)], \quad \phi(\eta = 0; r) = 1 \quad (23)$$

$$\frac{\partial f(\eta \rightarrow \infty; r)}{\partial \eta} = 0, \quad \theta(\eta \rightarrow \infty; r) = 0 = \phi(\eta \rightarrow \infty; r) \quad (24)$$

The symbols $\hbar \neq 0$ and $H \neq 0$ connote auxiliary functions while $r \in [0, 1]$ body-forth embedded parameter. The expressions for N_f , N_θ and N_ϕ which defined nonlinear operator are modeled as

$$N_f[f(\eta; r)] = \frac{\partial^3 f(\eta; r)}{\partial \eta^3} + f(\eta; r) \frac{\partial^2 f(\eta; r)}{\partial \eta^2} - 2 \left(\frac{\partial f(\eta; r)}{\partial \eta} \right)^2 \\ + We \left[\frac{3}{2} \left(\frac{\partial^2 f(\eta; r)}{\partial \eta^2} \right)^2 - 3 \frac{\partial f(\eta; r)}{\partial \eta} \frac{\partial^3 f(\eta; r)}{\partial \eta^3} + \frac{1}{2} f(\eta; r) \frac{\partial^4 f(\eta; r)}{\partial \eta^4} \right] \\ - 2P_s \frac{\partial f(\eta; r)}{\partial \eta} = 0 \quad (25)$$

$$N_\theta[f(\eta; r), \theta(\eta; r)] = \frac{\partial^2 \theta(\eta; r)}{\partial \eta^2} + Pr f(\eta; r) \frac{\partial \theta(\eta; r)}{\partial \eta} \\ - \frac{1}{2} \delta We Pr Ec \left[\frac{\partial f(\eta; r)}{\partial \eta} \left(\frac{\partial^2 f(\eta; r)}{\partial \eta^2} \right)^2 - f(\eta; r) \frac{\partial^2 f(\eta; r)}{\partial \eta^2} \frac{\partial^3 f(\eta; r)}{\partial \eta^3} \right] \\ + \frac{1}{2} Pr \lambda_e \left(f(\eta; r) \frac{df(\eta; r)}{d\eta} \frac{d\theta(\eta; r)}{d\eta} - (f(\eta; r))^2 \frac{d^2 \theta(\eta; r)}{d\eta^2} \right) \\ + Pr Ec \left(\frac{\partial^2 f(\eta; r)}{\partial \eta^2} \right)^2 + Pr Q \theta(\eta; r) = 0 \quad (26)$$

$$N_\phi[f(\eta; r), \phi(\eta; r)] = \frac{\partial^2 \phi(\eta; r)}{\partial \eta^2} + Sc f(\eta; r) \frac{\partial \phi(\eta; r)}{\partial \eta} \\ - R Sc \phi(\eta; r) = 0 \quad (27)$$

The functions $f(\eta; r)$, $\theta(\eta; r)$ and $\phi(\eta; r)$ approach $f_0(\eta)$, $\theta_0(\eta)$ and $\phi_0(\eta)$ when r varies between zero to one, to form $f(\eta)$, $\theta(\eta)$ and $\phi(\eta)$. The functions $f(\eta; r)$, $\theta(\eta; r)$ and $\phi(\eta; r)$ in Taylor series are

considered as

$$f(\eta; r) = f_0(\eta) + \sum_{m=1}^{\infty} f_m(\eta)r^m, \theta(\eta; r) = \theta_0(\eta) + \sum_{m=1}^{\infty} \theta_m(\eta)r^m$$

$$\phi(\eta; r) = \phi_0(\eta) + \sum_{m=1}^{\infty} \phi_m(\eta)r^m \quad (28)$$

Here,

$$f_m(\eta) = \frac{1}{m!} \frac{\partial^m f(\eta; r)}{\partial \eta^m}, \theta_m(\eta) = \frac{1}{m!} \frac{\partial^m \theta(\eta; r)}{\partial \eta^m}, \phi_m(\eta) = \frac{1}{m!} \frac{\partial^m \phi(\eta; r)}{\partial \eta^m}$$

The convergence of above equation (28) stands on \hbar . However, if \hbar is taken to give way for equation (28) to converge at $r = 1$, then

$$f(\eta) = f_0(\eta) + \sum_{m=1}^{\infty} f_m(\eta), \theta(\eta) = \theta_0(\eta) + \sum_{m=1}^{\infty} \theta_m(\eta)$$

$$\phi(\eta) = \phi_0(\eta) + \sum_{m=1}^{\infty} \phi_m(\eta) \quad (29)$$

The m th – order – deformation are modeled as

$$L_f[f_m(\eta) - \chi_m f_{m-1}(\eta)] = \hbar R_m^f(\eta),$$

$$L_\theta[\theta_m(\eta) - \chi_m \theta_{m-1}(\eta)] = \hbar R_m^\theta(\eta)$$

$$L_\phi[\phi_m(\eta) - \chi_m \phi_{m-1}(\eta)] = \hbar R_m^\phi(\eta) \quad (30)$$

$$f_m(\eta = 0; r = 0) = 0, \frac{\partial f_m(\eta = 0; r = 0)}{\partial \eta} = 0,$$

$$\frac{\partial \theta_m(\eta = 0; r = 0)}{\partial \eta} = -\gamma [1 + \theta_m(\eta = 0; r = 0)],$$

$$\phi_m(\eta = 0; r = 0) = 0 \quad (31)$$

$$\frac{\partial f_m(\eta \rightarrow \infty; r = 0)}{\partial \eta} = 0, \theta_m(\eta \rightarrow \infty; r = 0) = 0$$

$$\phi_m(\eta \rightarrow \infty; r = 0) = 0 \quad (32)$$

and

$$\begin{aligned}
 R_m^f(\eta) &= \frac{d^3 f_{m-1}(\eta)}{d\eta^3} + \sum_{n=0}^{m-1} f_n(\eta) \frac{d^2 f_{m-1-n}(\eta)}{d\eta^2} - 2 \sum_{n=0}^{m-1} \frac{df_n(\eta)}{d\eta} \frac{df_{m-1-n}(\eta)}{d\eta} \\
 &+ We \left[\frac{3}{2} \sum_{n=0}^{m-1} \frac{d^2 f_n(\eta)}{d\eta^2} \frac{d^2 f_{m-1-n}(\eta)}{d\eta^2} - 3 \sum_{n=0}^{m-1} \frac{df_n(\eta)}{d\eta} \frac{d^3 f_{m-1-n}(\eta)}{d\eta^3} \right] \\
 &+ We \left[\frac{1}{2} \sum_{n=0}^{m-1} f_n(\eta) \frac{d^4 f_{m-1-n}(\eta)}{d\eta^4} \right] - 2Ps \frac{df_{m-1}(\eta)}{d\eta} \quad (33)
 \end{aligned}$$

$$\begin{aligned}
 R_m^\theta(\eta) &= \frac{d^2 \theta_{m-1}(\eta)}{d\eta^2} + Pr \sum_{n=0}^{m-1} f_n(\eta) \frac{d\theta_{m-1-n}(\eta)}{d\eta} \\
 &+ PrEc \sum_{n=0}^{m-1} f_n(\eta) \frac{d^2 f_n(\eta)}{d\eta^2} \frac{d^2 f_{m-1-n}(\eta)}{d\eta^2} \\
 &- \frac{1}{2} \delta We Pr Ec \sum_{l=0}^{m-1} \frac{d^2 f_{m-1-l}(\eta)}{d\eta^2} \left(\sum_{j=0}^l \frac{d^2 f_{l-j}(\eta)}{d\eta^2} \frac{df_j(\eta)}{d\eta} \right) \\
 &- \frac{1}{2} \delta We Pr Ec \sum_{l=0}^{m-1} f_{m-1-l}(\eta) \left(\sum_{j=0}^l \frac{d^2 f_{l-j}(\eta)}{d\eta^2} \frac{d^3 f_j(\eta)}{d\eta^3} \right) \\
 &+ \frac{1}{2} Pr \lambda_e \sum_{l=0}^{m-1} f_{m-1-l}(\eta) \left(\sum_{j=0}^l \frac{df_{l-j}(\eta)}{d\eta} \frac{d\theta_j(\eta)}{d\eta} \right) \\
 &- \frac{1}{2} Pr \lambda_e \sum_{l=0}^{m-1} (f_{m-1-l}(\eta))^2 (f_{l-j}(\eta))^2 \left(\sum_{j=0}^l \frac{d^2 \theta_j(\eta)}{d\eta^2} \right) \\
 &+ Pr Q \theta_{m-1}(\eta) \quad (34)
 \end{aligned}$$

$$\begin{aligned}
 R_m^\phi(\eta) &= \frac{d^2 \phi_{m-1}(\eta)}{d\eta^2} + Sc \sum_{n=0}^{m-1} f_n(\eta) \frac{d\phi_{m-1-n}(\eta)}{d\eta} \\
 &- RSc \phi_{m-1}(\eta) \quad (35)
 \end{aligned}$$

$$X_m = 0 \text{ for } m \leq 1$$

$$X_m = 0 \text{ for } m > 1$$

the model general-solutions of above Eq. (30) are

$$f_m(\eta) = f_m(\eta)^* + C_1 + C_2 \exp(\eta) + C_3 \exp(-\eta) \quad (36)$$

$$\theta_m(\eta) = \theta_m(\eta)^* + C_4 + C_5 \exp(-\eta) \quad (37)$$

$$\phi_m(\eta) = \phi_m(\eta)^* + C_6 + C_7 \exp(-\eta) = 0 \quad (38)$$

3.2. CONVERGENCE OF THE (HAM) SOLUTION

Taking cognizant of the ideas of other researchers like Hayat *et al.* [21], Koriko *et al.* [22], Akinbo and Olajuwon[23-26], the convergence of the series solution of the models depend on non-zero auxiliary parameters ($\hbar_f, \hbar_\theta, \hbar_\phi$) which significantly controls the region at which the series solutions converge. Invoking $Q = 0.1$, $We = 0.1$, $\delta = 0.2$, $P_s = 0.1$, $Ec = 0.1$, $Pr = 0.72$, $\lambda_e = 0.1$, and $\gamma = 0.2$, the parallel region of \hbar - *curve*, which depict the convergences region of \hbar_f, \hbar_θ and \hbar_ϕ are selected as $\hbar_f \in [-2.7, -0.2]$, $\hbar_\theta \in [-3.7, -0.3]$ and $\hbar_\phi \in [-2.3, -0.2]$ (See Fig. (2)).

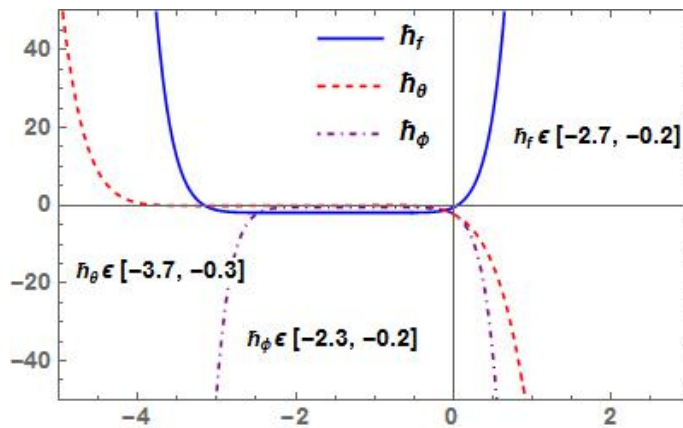


Fig. 2. $\hbar_{f,\theta,\phi}$ - *curves* for $f''(0), \theta'(0)$ and $\phi'(0)$ at 10th order of approximations

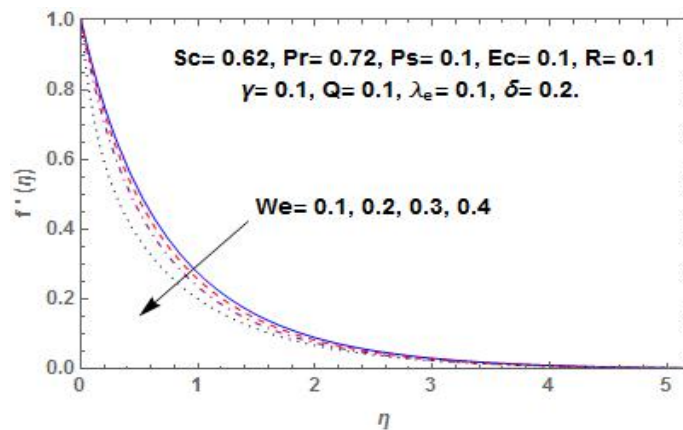


Fig. 3. Effect of We on $f'(0)$

4. DISCUSSION OF RESULTS

The significance of various dimensionless parameters are discussed here for more insight into the model.

Table 1. Convergence of solution with $Q = 0.1$, $We = 0.1$, $\delta = 0.2$, $Ps = 0.1$, $Ec = 0.1$, $Pr = 0.72$, $\lambda_e = 0.1$, and $\gamma = 0.2$.

<i>Order of Approximation</i>	$ f''(0) $	$ \theta'(0) $	$ \phi'(0) $
5	1.4659	0.1310	0.4754
10	1.4666	0.1376	0.4611
12	1.4667	0.1393	0.4595
14	1.4668	0.1408	0.4585
16	1.4668	0.1420	0.4579
18	1.4669	0.1431	0.4576
20	1.4669	0.1441	0.4575
22	1.4669	0.1450	0.4575
24	1.4669	0.1450	0.4575
26	1.4669	0.1451	0.4575
28	1.4669	0.1451	0.4575
30	1.4669	0.1451	0.4575

Table 1 elucidates convergence orders of the iterations in agreement with the far-field boundary conditions. Clearly from the table, the momentum equation converges at 18th-order of iterations while the concentration and energy equations follow suit at 20th and 26th-orders of iterations respectively.

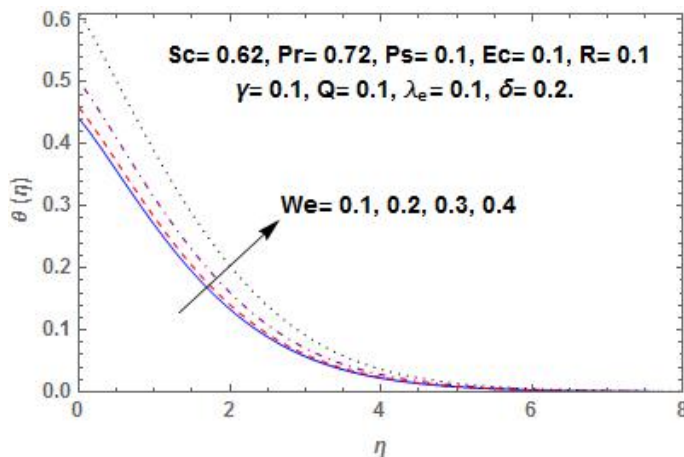


Fig. 4. Effect of We on $\theta(\eta)$

Fig. (3-4) illustrate the reaction of the local Weissenberg Number (We) on non-dimensional velocity $f'(0)$ and temperature $\theta(\eta)$. Various values of (We) give rise to viscoelasticity influence by virtue of tensile stress which thusly declines the motion of the fluid as well as momentum layer thickness. However, the reverse is the case for $\theta(\eta)$ which consequently strengthens thermal layer thickness.

The impact of porosity parameter (Ps) on velocity $f'(\eta)$ and temperature $\theta(\eta)$ are demonstrated in Fig. (5-6). A deeper hindrance is observed against the motion of the fluid which reduces the momentum boundary layer thickness. However, more heat is produced across the boundary layer which significantly improves $\theta(\eta)$ and brace-up thermal layer thickness.

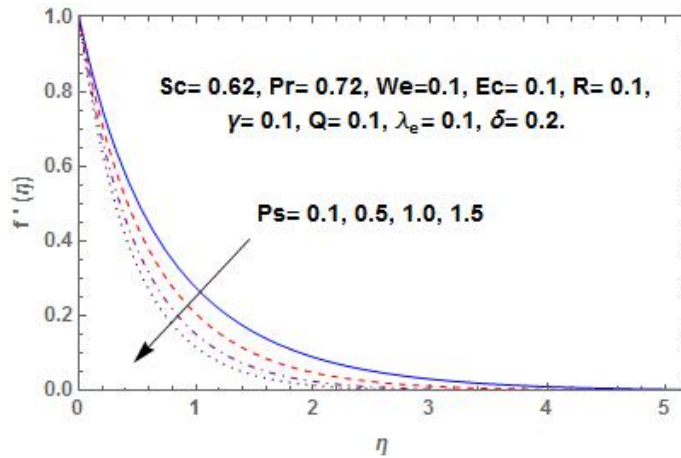


Fig. 5. Effect of Ps on $f'(\eta)$

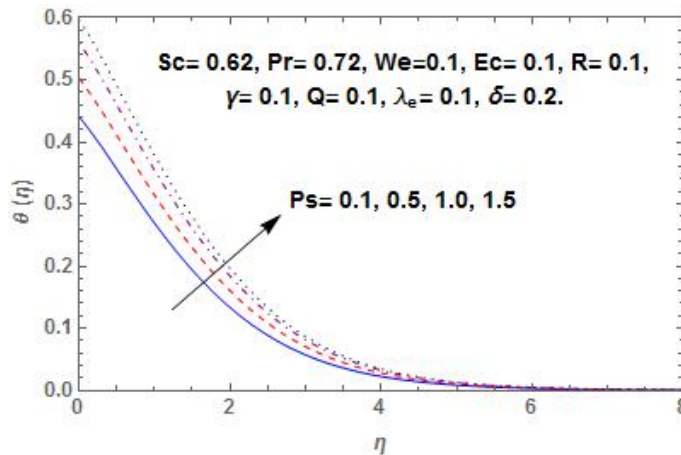


Fig. 6. Effect of Ps on $\theta(\eta)$

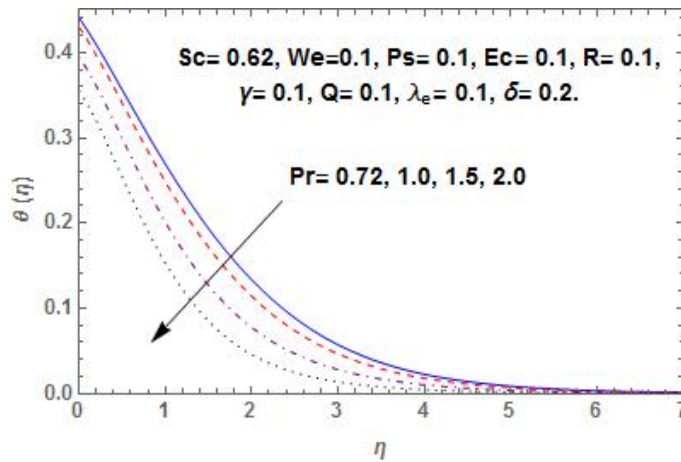


Fig. 7. Effect of Pr on $\theta(\eta)$

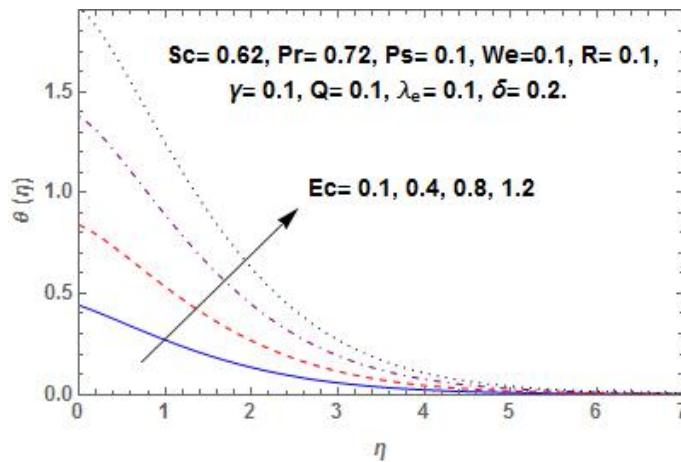


Fig. 8. Effect of Ec on $\theta(\eta)$

Fig. 7 depicts the behaviors of Prandtl number (Pr) on temperature $\theta(\eta)$. An increase in (Pr) limits conduction which obviously, corresponds to a lower thermal diffusivity that thusly reduces $\theta(\eta)$ and thins thermal boundary layer thickness. The behavior of Eckert number (Ec) on temperature field $\theta(\eta)$ is pictured in Fig. 8. Eckert number (Ec) expresses relationship between the conversions of kinetic energy to internal energy by work done against viscous stresses which makes the process to be irreversible. On this note, enhancement in (Ec) portrays improvement in conversion rate of kinetic energy to internal energy which consequently boosts the temperature field and its associated thermal boundary layer thickness (Koriko *et al.* [27]). The fluid near the surface gets heated as

(Ec) increases. This consequently magnifies the temperature field $\theta(\eta)$ due to the heat addition by means of frictional heating and boosts thermal boundary layer thickness. This outcome conformed with Abel and Begum [28]. The impact of Elastic-deformation (δ) depresses the dimensionless temperature $\theta(\eta)$ with an increase in (δ) of which its aftermath reduces thermal boundary layer thickness (See Fig. 9)

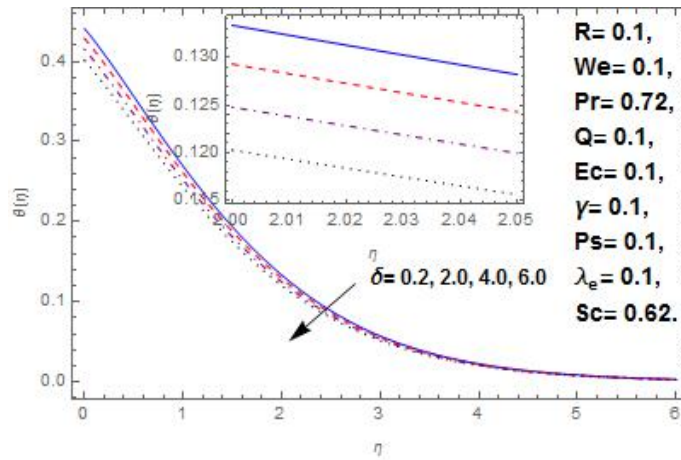


Fig. 9. Effect of δ on $\theta(\eta)$

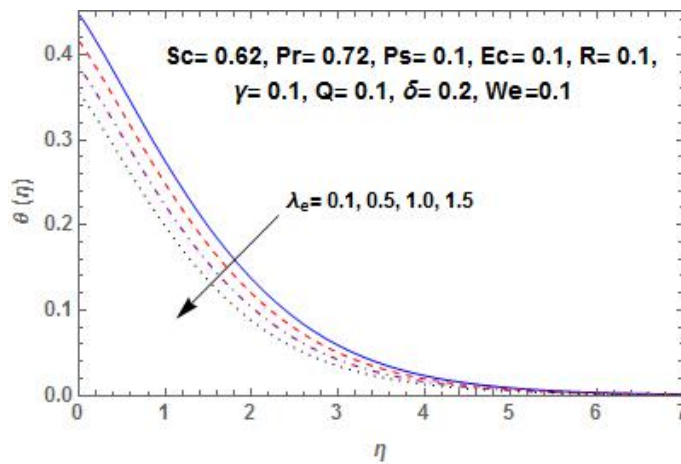


Fig. 10. Effect of λ_e on $\theta(\eta)$

Fig. 10 poses the significance of thermal relaxation time (λ_e) on the temperature profile. The temperature field $\theta(\eta)$ and thermal layer thickness thin with variation in thermal relaxation time (λ_e).

Indicating that materials particles crave for excessive time for the nearest particles on the bounding surface to experience heat.

Fig. 11 portrays the behaviors of conjugate parameter (γ) which expresses the strength of Newtonian heating on temperature field $\theta(\eta)$. The presence of ($\gamma > 0$) pioneer greater convective heating across the boundary layer which magnifies the temperature field and boosts thermal layer thickness. Fig. 12 elucidates the significance of Heat Generation ($Q > 0$)/Absorption ($Q < 0$) on non-dimensional temperature $\theta(\eta)$. An increase in Q amplifies the fluid molecules which results in an increase in $\theta(\eta)$ as well as thermal layer thickness.

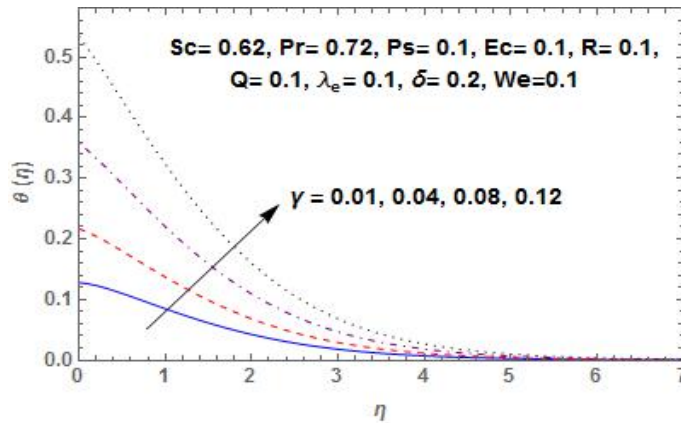


Fig. 11. Effect of γ on $\theta(\eta)$

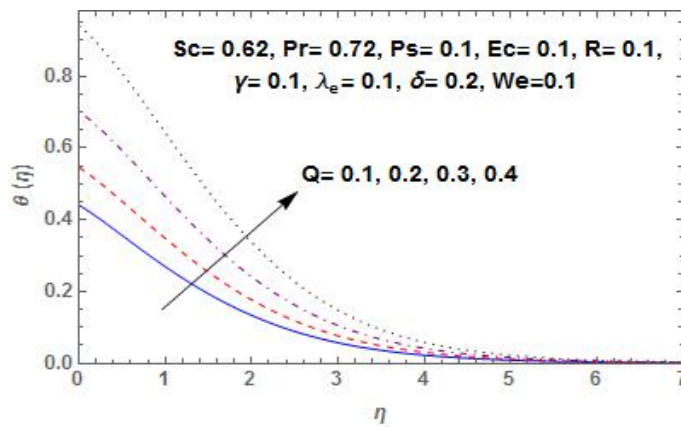


Fig. 12. Effect of Q on $\theta(\eta)$

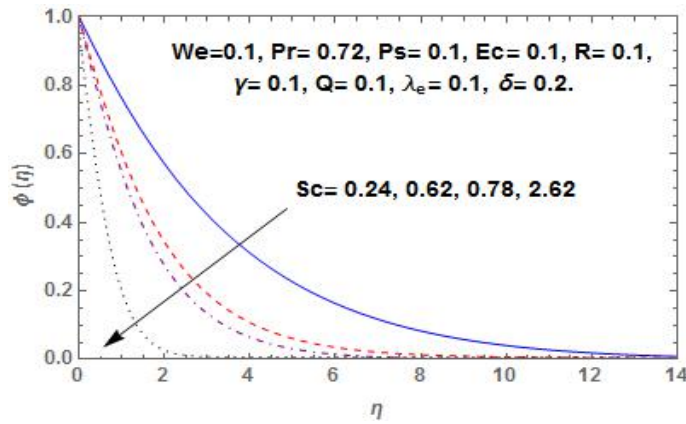


Fig. 13. Effect of Sc on $\phi(\eta)$

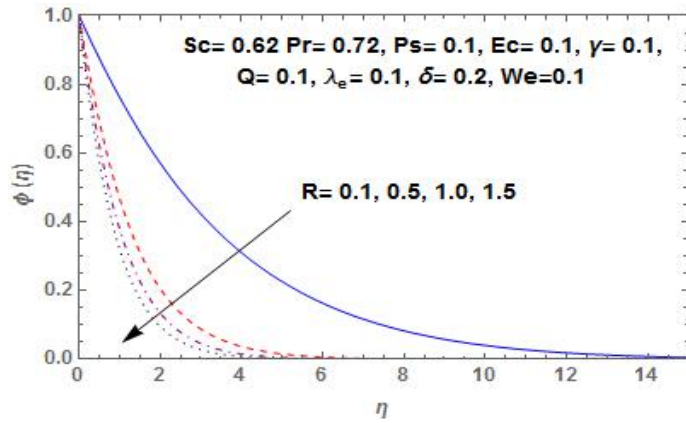


Fig. 14. Effect of R on $\phi(\eta)$

Various values of Schmidt number which varies from 0.24-2.62 for diffusing chemical species in the air, obviously decreases the mass diffusivity which decays the diffusion properties with aftermath reduction on concentration field $\phi(\eta)$ and its boundary layer thickness (See Fig. 13). Fig. 14 body-forth the impact of chemical reaction on non-dimensional concentration $\phi(\eta)$. As $R > 0$ the concentration buoyancy effect break-down, which consequently diminishes the concentration field $\phi(\eta)$ and thins concentration boundary layer thickness.

Table 2 reports numerically, the impact of We and Ps on local Skin-friction. Variation in We and Ps obviously posed negative values, indicating the presence of drag force on the fluid via the

plate. However, the skin-friction is an increasing property of We (Abegunrin *et al.* [29]) with a reverse phenomenon on Ps .

Table 2. Validation of the result/Significance of the embedded parameters on local Skin-friction.

<i>parameters</i>		<i>HAM</i>	<i>GWRM</i>
<i>We</i>	<i>Ps</i>	$Re_x^{\frac{1}{2}} Cf_x$	$Re_x^{\frac{1}{2}} Cf_x$
0.1	0.1	-0.953574	-0.953571
0.2		-0.487186	-0.487187
0.3		0.095326	0.095321
	0.5	-1.138849	-1.138867
	1.0	-1.333918	-1.333919

Table 3. Validation of the result/Significance of the embedded parameters on Nusselt number

<i>parameters</i>							<i>HAM</i>	<i>GWRM</i>
<i>We</i>	<i>Ec</i>	<i>Pr</i>	δ	γ	λ_e	<i>Q</i>	$-Re_x^{\frac{1}{2}} Nu_x$	$-Re_x^{\frac{1}{2}} Nu_x$
0.1	0.1	0.72	0.2	0.1	0.1	0.1	0.242325	0.242323
0.2							0.220969	0.220955
0.4							0.188078	0.188069
	0.4						0.175679	0.175676
	0.8						0.146269	0.146265
		1.0					0.309169	0.309166
		1.5					0.378475	0.378469
			2.0				0.246472	0.246470
			4.0				0.251164	0.251162
				0.01			0.066011	0.066010
				0.04			0.167788	0.167786
				0.08			0.225613	0.225611
					0.5		0.276276	0.276275
					1.5		0.322176	0.322168
						0.5	0.448594	0.448592
						1.5	0.315158	0.315155

Table 3 report the interactive impact of various parameters on the local Nusselt number. The surface heat is strengthening as Conjugate parameter, thermal relaxation time, Prandtl number and Elastic-deformation improved which consequently escalate the

heat transfer rate. However, opposite phenomena are observed as local Weissenberg number, Eckert number, and heat generation/absorption gain strength.

Table 4. Validation of the result/Significance of the embedded parameter on local Sherwood number

<i>parameter</i>		<i>HAM</i>	<i>GWRM</i>
<i>Sc</i>	<i>R</i>	$Re_x^{\frac{1}{2}} C f_x$	$Re_x^{\frac{1}{2}} C f_x$
0.24		0.263966	0.263831
0.62		0.474003	0.474356
0.78		0.549135	0.549139
	0.5	0.416780	0.416676
	1.0	0.548601	0.548685

Table 4 numerically reveals the behaviors of Sc and R on local Sherwood number. Various values of Sc and R are found to improve the Sherwood number, which consequently strengthens the surface mass transfer.

5. CONCLUDING REMARKS

In this report, the interactive impact of Cattaneo-Christov heat flux model, coupled with the influence of viscous dissipation, heat generation/absorption and chemical reaction on the flow of Walters' B fluid in the presence of Newtonian heating has been tackled via Homotopy Analysis Method and the following key point are raised among others.

- The result via Homotopy Analysis method perfectly agreed with another method when compared with Galerkin Weighted Residual.
- Various values of Heat Generation ($Q > 0$) amplifies the fluid molecules, which brace-up the temperature field and boosts the associated layer thickness.
- The local Sherwood number is strengthened with various values of Schmidt number and chemical reaction and this consequently improves the surface mass transfer.
- The temperature field declined over various values of thermal relaxation time, indicating that materials particles require additional time to experience the heat at the closet particles.
- Different values of local Weissenberg Number escalate viscoelasticity intensity via tensile stress, which slow-down the

motion of fluid whose aftermath impact reduces momentum boundary layer thickness.

ACKNOWLEDGEMENTS

The author would like to thank the anonymous referee whose comments improved the original version of this manuscript.

NOMENCLATURE

Q	Heat generation/Absorption
We	Local Weissenberg Number
Pr	Prandtl number
Ec	Eckert number
λ_e	Thermal relaxation time
Ps	Porosity parameter
Sc	Schmidt number
D	Mass diffusivity
γ	Conjugate parameter for Newtonian heating
α	thermal diffusivity
η	Similarity variable
θ	dimensionless temperature
ν	kinematic viscosity
ρ	density
C_p	specific heat at constant pressure
h_s	heat transfer coefficients

REFERENCES

- [1] T. Hayat, M. Farooq, A. Alsaedi, F. Al-Solamy, *Impact of Cattaneo-Christov heat flux in the flow over a stretching sheet with variable thickness*. Aip Advances **5**, 087159-12, 2015.
- [2] T. Hayat, M. I. Khan, M. Waqas, A. Alsaedi, *On CattaneoChristov heat flux in the flow of variable thermal conductivity Eyring-Powell fluid*, Results in Physics, **7**, 446-450, 2017.
- [3] T. Hayat, I. M. Khan, M. Farooq, A. Alsaedi, I. M. Khan, *Thermally stratified stretching flow with CattaneoChristov heat flux*, International Journal of Heat and Mass Transfer, **106**, 289294, 2017.
- [4] A. S. Dogonchi, D. D. Ganji, *Effect of CattaneoChristov heat flux on buoyancy MHD nanofluid flow and heat transfer over a stretching sheet in the presence of Joule heating and thermal radiation impacts*, Indian Journal of Physics, **96**, 757-766, 2017.
- [5] S. Shah, S. Hussain, M. Sagheer, *MHD effects and heat transfer for the UCM fluid along with Joule heating and thermal radiation using Cattaneo-Christov heat flux model*, Aip Advances, **6**, 085103-11, 2016.
- [6] M. Mustafa, *Cattaneo-Christov heat flux model for rotating flow and heat transfer of upper-convected Maxwell fluid*, Aip Advances, **5**, 047109-10, 2015.

- [7] S. Han, L. Zheng, C. Li, X. Zhang, *Coupled flow and heat transfer in viscoelastic fluid with Cattaneo-Christov heat flux model*, Applied Mathematics Letters, 38, 8793, 2014
- [8] K. A. Kumar, J. V. R. Reddy, V. Sugunamma, N. Sandeep, *Magnetohydrodynamic Cattaneo-Christov flow past a cone and a wedge with variable heat source/sink*, Alexandria Engineering Journal, 57, 435-443, 2018.
- [9] B. Mahanthesh, B. J. Gireesha, C.S.K. Raju, *Cattaneo-Christov heat flux on UCM nanofluid flow across a melting surface with double stratification and exponential space dependent internal heat source*, Informatics in Medicine Unlocked, 9, 26-34, 2017
- [10] M. E. Ali, N. Sandeep, *Cattaneo-Christov model for radiative heat transfer of magnetohydrodynamic Casson-Ferrofluid: A numerical study*, Results in Physics, 7, 2130, 2017.
- [11] S. Nadeem, A. Ahmad, N. Muhammad, *Cattaneo-Christov flux in the flow of a viscoelastic fluid in the presence of Newtonian heating*, Journal of Molecular Liquids, 237, 180184, 2017
- [12] M. Khan, W. A. Khan, *Three-dimensional flow and heat transfer to burgers fluid using Cattaneo-Christov heat flux model*, Journal of Molecular Liquids, 221, 651657, 2016
- [13] A. S. Dogonchi, D. D. Ganji, *Impact of Cattaneo-Christov heat flux on MHD nanofluid flow and heat transfer between parallel plates considering thermal radiation effect*, Journal of the Taiwan Institute of Chemical Engineers 0 0 0, 112, 2017.
- [14] F. M. Abbasi, S. A. Shehzad, *Heat transfer analysis for three-dimensional flow of Maxwell fluid with temperature dependent thermal conductivity: Application of Cattaneo-Christov heat flux model*, Journal of Molecular Liquids, 220, 848854, 2016
- [15] L. Liu, L. Zheng, F. Liu, X. Zhang, *Heat conduction with fractional Cattaneo-Christov upper-convective derivative flux model. International Journal of Thermal Sciences*, 112, 421-426, 2017.
- [16] K.A. Kumar, J.V.R. Reddy, V. Sugunamma, N. Sandeep, *MHD Carreau Fluid Flow Past a Melting Surface with Cattaneo-Christov Heat Flux*. Trends in Mathematics, 325-336, 2019. doi.org/10.1007/978-3-030-01123-9_32.
- [17] M. M. Nandeppanavar, S. M. Abel, J. Tawade, *Heat transfer in a Walter, s liquid B fluid over an impermeable stretching sheet with non-uniform heat source/sink and elastic deformation*, Communications in Nonlinear Science and Numerical Simulation, 15, 1791-1802, 2010.
- [18] T. Hayat, A. Shafiq, M. Mustafa, A. Alsaedi, *Boundary-Layer Flow of Walters B Fluid with Newtonian Heating*, Z. Naturforsch, 70(5)a, 333341, 2015
- [19] S. K. Khan, *Boundary layer viscoelastic fluid flow over an exponentially stretching sheet*, International Journal of Applied Mechanics and Engineering 11, 321-335, 2006.
- [20] M. M. Rashidi, B. Rostami, N. Freidoonimehr, S. Abbasbandy, *Free convective heat and mass transfer for MHD fluid flow over a permeable vertical stretching sheet in the presence of the radiation and buoyancy effects*, Ain Shams Engineering Journal, 5, 901-912, 2014.
- [21] T. Hayat, Q. Sajid, A. Ahmed, A. Bashir, *Magnetohydrodynamic (MHD) nonlinear convective flow of Walters-B nanofluid over a nonlinear stretching sheet with variable thickness*, International Journal of Heat and Mass Transfer, 110, 506514, 2017.
- [22] O. K. Koriko, I. L. Animasaun, A. J. Omowaye, T. Oreyeni, *The combined influence of nonlinear thermal radiation and thermal stratification on the dynamics*

- of micropolar fluid along a vertical surface*, Multidiscipline Modeling in Materials and Structures, 15, 133-155, 2018
- [23] B. J. Akinbo, B. I. Olajuwon, *Impact of radiation and chemical reaction on stagnation-point flow of Hydromagnetic Walters' B fluid with Newtonian heating*, International Communications in Heat and Mass Transfer, 121, 105115, 2021.
- [24] B. J. Akinbo, B. I. Olajuwon, *Heat transfer analysis in a hydromagnetic Walters' B fluid with elastic deformation and Newtonian heating*, Heat Transfer, 50, 2033-2048, 2021.
- [25] B. J. Akinbo, B. I. Olajuwon, *Homotopy analysis investigation of heat and mass transfer flow past a vertical porous medium in the presence of heat source* International Journal of Heat and Technology, 37(3): 899-908, 2019.
- [26] B. J. Akinbo, B. I. Olajuwon, *Radiation and thermal-diffusion interaction on stagnation-point flow of Walters' B fluid toward a vertical stretching sheet* International Communications in Heat and Mass Transfer, 126, 105471, 2021.
- [27] O. K. Koriko, K. S. Adegbe, N. A. Shah, I. L. Animasaun M. A. Olotu, *Numerical solutions of the partial differential equations for investigating the significance of partial slip due to lateral velocity and viscous dissipation: The case of blood-gold Carreau nanofluid and dusty fluid* Numerical Methods for Partial Differential Equations, 37, 129, 2021.
- [28] M. S. Abel, G. Begum, *Heat Transfer in MHD Viscoelastic Fluid Flow on Stretching Sheet with Heat Source/Sink, Viscous Dissipation, Stress Work, and Radiation for the Case of Large Prandtl Number*, Chemical Engineering Communications, 195, 15031523, 2008.
- [29] O. A. Abegunrin, S. O. Okhuevbie, I. L. Animasaun, *Comparison between the flow of two non-Newtonian fluids over an upper horizontal surface of paraboloid of revolution: Boundary layer analysis*, Alexandria Engineering Journal, 55(3), 1915-1929, 2016.

DEPARTMENT OF MATHEMATICS, FEDERAL UNIVERSITY OF AGRICULTURE, ABEOKUTA, NIGERIA.

E-mail address: akinbomaths@gmail.com

DEPARTMENT OF MATHEMATICS, FEDERAL UNIVERSITY OF AGRICULTURE, ABEOKUTA, NIGERIA.

E-mail address: shola1@gmail.com